STUDYING THE INFLUENCE OF ROLL AND PITCH DYNAMICS IN OPTIMAL ROAD-VEHICLE MANEUVERS

Kristoffer Lundahl*, Karl Berntorp†, Björn Olofsson†, Jan Åslund*, Lars Nielsen*

* Department of Electrical Engineering,
Linköping University,
SE–581 83 Linköping, Sweden,
firstname.lastname@liu.se

† Department of Automatic Control,
Lund University,
SE–221 00 Lund, Sweden,
firstname.lastname@control.lth.se

Abstract

A comparative analysis shows how vehicle motion models of different complexity, capturing various characteristics, influence the solution when used in time-critical optimal maneuvering problems. Vehicle models with combinations of roll and pitch dynamics as well as load transfer are considered, ranging from a single-track model to a double-track model with roll and pitch dynamics combined with load transfer. The optimal maneuvers in a 90°-turn and a double lane-change scenario are formulated as minimum-time optimization problems, and are solved using numerical optimization software. The results obtained with the different models show that variables potentially important for safety systems, such as the yaw rate, slip angle, and geometric path, are qualitatively the same. Moreover, the numeric differences are mostly within a few percent. The results also indicate that although input torques differ about 50–100 % for certain parts of the maneuver between the most and least complex model considered, the resulting vehicle motions obtained are similar, irrespective of the model. Our main conclusion is that this enables the use of low-order models when designing the onboard optimization-based safety systems of the future.

1. INTRODUCTION

With recent advancements in optimization technology and software, new approaches unfold for the development of active vehicle safety systems and driver assistance technologies, see, *e.g.*, [1]. The solution to an optimal control problem can give valuable insight into the performance capabilities of the system being investigated. Also, it can be used as an inspiration for new control strategies. The solution to the optimization problem will depend on the choice of model configurations and optimization objectives, investigated in [2] and [3]. There, we developed an optimization methodology with special emphasis on tire modeling and uncertain road-surfaces, and this work continues the development towards more complex chassis models.

Motivated by the above, this study investigates the similarities and differences in the solutions obtained when several vehicle chassis models, capturing different dynamic properties such as roll and pitch dynamics with load transfer, are employed in optimal maneuvering problems. The aim is to perform a comparative study on how different vehicle motion models affect the optimal control solution in certain critical situations. The long-term goal of this work is real-time control. Hence, the models investigated are fairly simplistic compared to models traditionally employed for vehicle simulation purposes. For example, detailed suspension kinematics and gear dynamics have been neglected. One motivation for this is that the models are to be used together with dynamic optimization algorithms, requiring twice continuously differentiable functions in the model description. In addition, and perhaps more importantly, we are interested in investigating what characteristics of a maneuver that can be captured with this kind of models.

Optimal control of vehicles has been investigated previously in literature, see [1, 4, 5, 6] for a few examples. Further, in [7, 8] an optimization problem for over-actuated vehicles is solved using similar software as used in this paper. A majority of the work in these references focus on a specific vehicle and tire model. Thus, to the best of our knowledge, no comprehensive approach to perform comparisons of different chassis models in an optimization scenario has been made, which motivates the study presented here.

The evaluation of the models is performed on two different maneuvering problems: A 90°-turn and a double lane-change situation, where the objective is to minimize the execution time of the maneuver. This formulation is one example of how to trigger a critical situation where the vehicle is performing at its very limit in terms of maneuvering.

2. MODELING

The emphasis in the vehicle modeling is on the chassis dynamics. Five different chassis models of various complexity are considered. The wheel dynamics and tire force modeling are the same in the five cases, where the former is expressed by a first-order rotational dynamic system. The tire forces are described by Pacejka's Magic Formula tire model in combination with weighting functions [9] for modeling combined longitudinal and lateral slip.

2.1 Chassis Models

The single-track (ST) model [10, 11], illustrated in Figure 1, is used as a basis model for the vehicle motion modeling. The left and right wheels on each axle are lumped together, and the model has two translational and one rotational degrees of freedom. The model dynamics are

$$\dot{v}_x - v_y\dot{\psi} = \frac{1}{m}(F_{x,f}\cos(\delta) + F_{x,r} - F_{y,f}\sin(\delta)), \tag{1}$$

$$\dot{v}_y + v_x\dot{\psi} = \frac{1}{m}(F_{y,f}\cos(\delta) + F_{y,r} + F_{x,f}\sin(\delta)), \tag{2}$$

$$I_{zz}\ddot{\psi} = l_f F_{y,f}\cos(\delta) - l_r F_{y,r} + l_f F_{x,f}\sin(\delta), \tag{3}$$

where m is the total vehicle mass, I_{zz} is the vehicle inertia about the z-axis, $\dot{\psi}$ is the yaw rate, δ is the steer angle, v_x, v_y are the longitudinal and lateral velocities at the center of gravity, l_f, l_r are the distances from the center of gravity to the front and rear wheel base, and F_x, F_y are the longitudinal and lateral tire forces acting at the front and rear wheels. The nominal normal force resting on the respective wheel is given by

$$F_{z0,f} = mg\frac{l_r}{l}, \quad F_{z0,r} = mg\frac{l_f}{l}, \tag{4}$$

where g is the constant of gravity and $l = l_f + l_r$.

Four extensions of the ST model are considered in this study:

- Single-track model with roll dynamics (ST-roll), where an additional degree of freedom about the x-axis is included.
- Single-track model with pitch dynamics—*i.e.*, an additional degree of freedom about the y-axis—and longitudinal load transfer (ST-pitch).
- Double-track model with roll dynamics and lateral load transfer (DT-roll).
- Double-track model with roll and pitch dynamics and both longitudinal and lateral load transfer (DT-roll-pitch).

In the double-track models, each of the four wheels are modeled separately. In Figure 2, the DT-roll-pitch model is illustrated, with the roll angle ϕ and the pitch angle θ. The chassis rotational motion in the roll and pitch directions is characterized by the vehicle chassis inertias I_{xx} and I_{yy}, respectively. Further, in the derivation of the models it was assumed that the suspension system of the vehicle can be modeled with a spring-damper system. Consequently, the moment produced by the suspension system in the roll direction is given by

$$\tau_\phi = (K_{\phi,f} + K_{\phi,r})\phi + (D_{\phi,f} + D_{\phi,r})\dot{\phi}, \tag{5}$$

and correspondingly in the pitch direction according to

$$\tau_\theta = K_\theta\theta + D_\theta\dot{\theta}, \tag{6}$$

where K and D are model parameters for the stiffness and damping, respectively. For the derivation and complete dynamic equations for DT-roll-pitch, see [12]. The dynamic equations for the longitudinal load transfer are given by

$$F_{z,f}l_f - F_{z,r}l_r = K_\theta\theta + D_\theta\dot{\theta}, \quad \sum_{i=f,r} F_{z,i} = mg, \tag{7}$$

for ST-pitch, where the time-dependent normal forces $F_{z,f}$ and $F_{z,r}$ have been introduced. The relation (7) is also valid for DT-roll-pitch with the substitution $F_{z,f} = F_{z,1} + F_{z,2}$ and $F_{z,r} = F_{z,3} + F_{z,4}$. The lateral load transfer is determined by the relations

$$-w(F_{z,1} - F_{z,2}) = K_{\phi,f}\phi + D_{\phi,f}\dot{\phi}, \tag{8}$$

$$-w(F_{z,3} - F_{z,4}) = K_{\phi,r}\phi + D_{\phi,r}\dot{\phi}, \tag{9}$$

where w is defined in Figure 2.

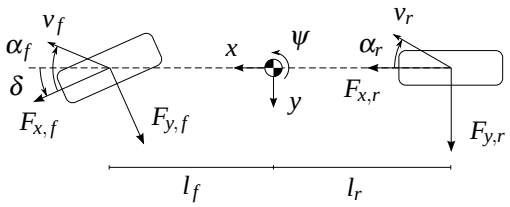

Figure 1 Basic single-track model.

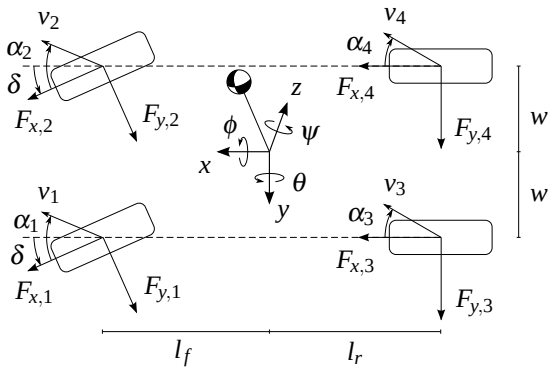

Figure 2 Double-track model with roll and pitch dynamics.

2.2 Wheel and Tire Dynamics

The wheel dynamics is formulated as a first-order system with the wheel angular velocity ω as the state and the driving and braking torques T acting on the wheels defined as inputs, according to

$$T_i - I_w\dot{\omega}_i - F_{x,i}R_w = 0,\ i = f,r \text{ or } 1,2,3,4, \tag{10}$$

where I_w is the wheel inertia and R_w is the wheel radius. The longitudinal slip κ and the slip angle α are introduced following [9], and are given by

$$\kappa_i = \frac{R_w\omega_i - v_{x,i}}{v_{x,i}}, \tag{11}$$

$$\dot{\alpha}_i\frac{\sigma}{v_{x,i}} + \alpha_i = -\arctan\left(\frac{v_{y,i}}{v_{x,i}}\right), \quad i = f,r \text{ or } 1,2,3,4, \tag{12}$$

where σ is the relaxation length and $v_{x,i}$, $v_{y,i}$ are the translational velocities resolved in the wheel frames. Note that Figures 1–2 depict the static slip angles, describing a purely geometric relation, in contrast to the dynamic slip angles in (12). The vehicle and wheel model parameters in (1)–(12) used in this study are specified in Table 1.

The tire forces are modeled by Pacejka's Magic Formula in combination with weighting functions [9] for modeling the combined longitudinal and lateral slip. The longitudinal and lateral tire forces, F_x and F_y, read

$$F_{x0,i} = \mu_x F_{z,i}\sin(C_{x,i}\arctan(B_{x,i}\kappa_i - E_{x,i}(B_{x,i}\kappa_i - \arctan B_{x,i}\kappa_i))), \tag{13}$$
$$B_{x\alpha,i} = B_{x1,i}\cos(\arctan(B_{x2,i}\kappa_i)), \tag{14}$$
$$G_{x\alpha,i} = \cos(C_{x\alpha,i}\arctan(B_{x\alpha,i}\alpha_i)), \tag{15}$$
$$F_{x,i} = F_{x0,i}G_{x\alpha,i}, \tag{16}$$
$$F_{y0,i} = \mu_y F_{z,i}\sin(C_{y,i}\arctan(B_{y,i}\alpha_i - E_{y,i}(B_{y,i}\alpha_i - \arctan B_{y,i}\alpha_i))), \tag{17}$$
$$B_{y\kappa,i} = B_{y1,i}\cos(\arctan(B_{y2,i}\alpha_i)), \tag{18}$$
$$G_{y\kappa,i} = \cos(C_{y\kappa,i}\arctan(B_{y\kappa,i}\kappa_i)), \tag{19}$$
$$F_{y,i} = F_{y0,i}G_{y\kappa,i},\ i = f,r \text{ or } 1,2,3,4, \tag{20}$$

where μ_x, μ_y are the longitudinal and lateral friction coefficients and B, C, E are model parameters. In Table 2 the tire model parameters in (13)–(20) used in this study are provided. The parameters were derived from [9] and correspond to a tire on dry asphalt. Further, the state variables for the respective vehicle and wheel model configuration are summarized in Table 3.

3. OPTIMIZATION

The models presented in the previous section are formulated as differential-algebraic equation systems according to $\dot{x}(t) = G(x(t),y(t),u(t))$, where x is the state vector, y are the algebraic variables, and u is the input signal vector. The time-dependency of the variables will be implicit in the rest of the paper. The wheel driving and braking torques, $T = \begin{pmatrix} T_f & T_r \end{pmatrix}$, as well as the steer angle δ of the front wheels are considered as inputs. For simplicity we assume that the front wheels have the same steer angle in the double-track models. To allow an equitable comparison with the single-track models, the double-track models only have two wheel-torque inputs as well, which are equally distributed between the wheels at the respective axle, *i.e.*, $T_1 = T_2 = T_f/2$ and $T_3 = T_4 = T_r/2$, where T_1, T_2, T_3, and T_4 are the corresponding wheel torques for wheel 1–4. Further, the tire-force model is written

Table 1 Vehicle and wheel parameters in (1)–(12).

Notation	Value	Unit
l_f	1.3	m
l_r	1.5	m
w	0.8	m
m	2 100	kg
I_{xx}	765	kgm^2
I_{yy}	3 477	kgm^2
I_{zz}	3 900	kgm^2
R_w	0.3	m
I_w	4.0	kgm^2
σ	0.3	m
g	9.82	ms^{-2}
h	0.5	m
$K_{\phi,f}, K_{\phi,r}$	89 000	Nm(rad)$^{-1}$
$D_{\phi,f}, D_{\phi,r}$	8 000	Nms(rad)$^{-1}$
K_θ	363 540	Nm(rad)$^{-1}$
D_θ	30 960	Nms(rad)$^{-1}$

Table 2 Tire model parameters in (13)–(20).

Notation	Front	Rear
μ_x	1.20	1.20
B_x	11.7	11.1
C_x	1.69	1.69
E_x	0.377	0.362
μ_y	0.935	0.961
B_y	8.86	9.30
C_y	1.19	1.19
E_y	-1.21	-1.11
$C_{x\alpha}$	1.09	1.09
B_{x1}	12.4	12.4
B_{x2}	-10.8	-10.8
$C_{y\kappa}$	1.08	1.08
B_{y1}	6.46	6.46
B_{y2}	4.20	4.20

Table 3 State variables for the different vehicle chassis model configurations, including wheel dynamics.

Model	Notation	States
Single-track	ST	$v_x, v_y, \dot{\psi}, \omega_f, \omega_r, \alpha_f, \alpha_r$
Single-track with roll dynamics	ST-roll	$v_x, v_y, \dot{\psi}, \dot{\phi}, \omega_f, \omega_r, \alpha_f, \alpha_r$
Single-track with pitch dynamics	ST-pitch	$v_x, v_y, \dot{\psi}, \dot{\theta}, \omega_f, \omega_r, \alpha_f, \alpha_r$
Double-track with roll dynamics	DT-roll	$v_x, v_y, \dot{\psi}, \dot{\phi}, \omega_1, \omega_2, \omega_3, \omega_4, \alpha_1, \alpha_2, \alpha_3, \alpha_4$
Double-track with roll and pitch	DT-roll-pitch	$v_x, v_y, \dot{\psi}, \dot{\phi}, \dot{\theta}, \omega_1, \omega_2, \omega_3, \omega_4, \alpha_1, \alpha_2, \alpha_3, \alpha_4$

as the equation system $h(x,y,u) = 0$. The chassis and tire dynamics are implemented using the modeling language Modelica [13]. The optimization problem is formulated over the time horizon $t \in [0, t_f]$. The objective of the optimization is to minimize the final time t_f of the maneuver. Accordingly, the dynamic optimization problem to be solved is written as:

$$\begin{aligned}
&\text{minimize} && t_f && (21)\\
&\text{subject to} && T_{i,\min} \le T_i \le T_{i,\max},\ i = f,r, && (22)\\
& && |\delta| \le \delta_{\max}, \quad |\dot{\delta}| \le \dot{\delta}_{\max}, && (23)\\
& && x(0) = x_0, \quad y(0) = y_0, && (24)\\
& && x(t_f) = x_{t_f}, \quad y(t_f) = y_{t_f}, && (25)\\
& && f(X_p, Y_p) \le 0, && (26)\\
& && \dot{x} = G(x,y,u), \quad h(x,y,u) = 0, && (27)
\end{aligned}$$

where x_0, y_0 are the initial conditions for the differential states and algebraic variables, x_{t_f}, y_{t_f} are the desired values at the final time $t = t_f$, and (X_p, Y_p) is the position of the center of gravity of the vehicle. In practice, the initial and final conditions are only applied to a subset of the model variables. Further, $f(X_p, Y_p)$ is a mathematical description of the road constraint for the center of gravity of the vehicle for the respective maneuver. These constraints are formulated as super-ellipses with different radii and degrees in the XY-plane.

The continuous-time optimal control problem (21)–(27) is solved for each model and maneuver using the open-source software JModelica.org [14], according to the method presented in [2]. In particular, the continuous-time optimization problem is discretized using direct collocation methods [15], and the resulting discrete-time nonlinear optimization problem (NLP) is solved numerically using the state-of-the-art interior-point solver Ipopt [16]. The Jacobian and the Hessian related to the problem are required in the iterative numerical optimization procedure. Considering the complexity of the employed chassis and tire models, exact calculation of these quantities with automatic differentiation [17] significantly reduces convergence times and increases numerical stability compared to the case with numerical approximations. For further details on the solution methodology, see [2].

4. RESULTS

The minimum-time optimization problem (21)–(27) was solved for the 90°-turn and the double lane-change maneuver. The solution of the problem was determined for each of the vehicle models presented in Section 2. The steer angle and steer rate-of-change were limited to $\delta_{\max} = 30$ deg and $\dot{\delta}_{\max} = 60$ deg/s, respectively, corresponding to reasonable driver limitations. The lower wheel torque limitations were set to $T_{f,\min} = T_{r,\min} = -\mu_{x,f} mg$. The upper wheel torque limits were set to $T_{f,\max} = 0$ and $T_{r,\max} = \mu_{x,r} F_{z0,r}$, which implies a rear-wheel driven vehicle. The choice of torque limitations originates from that the maximum braking torque that can be applied on the wheels is significantly larger than the corresponding acceleration torque. Further, the driving torque limit was set to prevent excessive wheel spin equivalent to large slip ratios. This is motivated since the employed empirical tire models are based on tire force measurements that for experimental reasons are only possible to obtain for a limited area in the α-κ plane. In addition, the wheel velocities were limited to be nonnegative, since solutions with wheel backspin are not desired.

4.1 Optimal Maneuver in the 90°-Turn

In the turn maneuver, the vehicle start position was set to $(X_{p,0}, Y_{p,0}) = (37.5, 0)$ m, *i.e.*, in the lower right corner in Figure 3. The initial velocity was $v_0 = 70$ km/h and the vehicle was aligned with the road direction, $\psi_0 = \pi/2$. The target vehicle position was set to $(X_{p,t_f}, Y_{p,t_f}) = (0, 37.5)$ m, where the vehicle heading was in the road direction, $\psi_{t_f} = \pi$. The computed optimal maneuvers for the different vehicle chassis models in the 90°-turn are presented in Figure 3. The variable v represents the absolute vehicle velocity and β is the body-slip angle, defined as

$$\beta = \arctan\left(\frac{v_y}{v_x}\right).$$

Figure 4 shows the sum of the longitudinal and lateral tire forces resolved in the road-surface plane. Also visualized is the nominal yaw moment M_Z generated from the tire forces, *i.e.*, the moment about an axis orthogonal to the road. These quantities are visualized as function of the driven distance s for comparability reasons. Figures 5–6 show the *Force-Slip (FS)-diagrams*—as first introduced in [2]—for ST and DT-roll-pitch. Here the normalized resultant tire-force, defined as

$$F_{i,res} = \frac{\sqrt{F_{x,i}^2 + F_{y,i}^2}}{F_{z,i}}, \quad i = f, r \text{ or } 1, 2, 3, 4,$$

is visualized as a surface, varying over α and κ. The corresponding time-optimal solution is drawn on this surface, as well as projected underneath in the α-κ plane. In Table 4, the execution times for the maneuver for the respective model are specified. The execution times vary 4 % at most, which occurs between ST-pitch and DT-roll. However, no significant differences between the five chassis models considered in this study are observed.

Similarities Between the Solutions

The first observation when investigating the results in Figure 3 is that the solutions practically coincide for several variables, being ϕ, θ, $\dot{\psi}$, and β. This implies that variables often utilized in safety systems to indicate maneuvering instability are invariant to model complexity, at least for the models considered here. The geometric trajectories shown in the upper left plot of Figure 3 are also similar. The largest deviations of the geometric trajectories, which occur between ST-pitch and DT-roll during the exit phase, are approximately 15 % of the road width. However, the differences between ST and DT-roll-pitch are minor throughout the maneuver.

As seen in Figure 4, F_Y and M_Z are similar, with only minor quantitative differences between the models. This observation can also be deduced from the tire force plots in Figure 3 and is important considering that M_Z is used as a high-level input in several safety systems, such as in yaw-rate controllers and rollover-prevention systems. There are larger numeric discrepancies in F_X, at least during shorter periods of the maneuver. In a physical setup, however, model parameters such as the friction coefficients, vehicle mass, and tire parameters are uncertain. Thus, for safety

Table 4 Time for executing the maneuver for each model configuration in the 90°-turn.

Model	Execution time
ST	4.27 s
ST-roll	4.27 s
ST-pitch	4.20 s
DT-roll	4.37 s
DT-roll-pitch	4.34 s

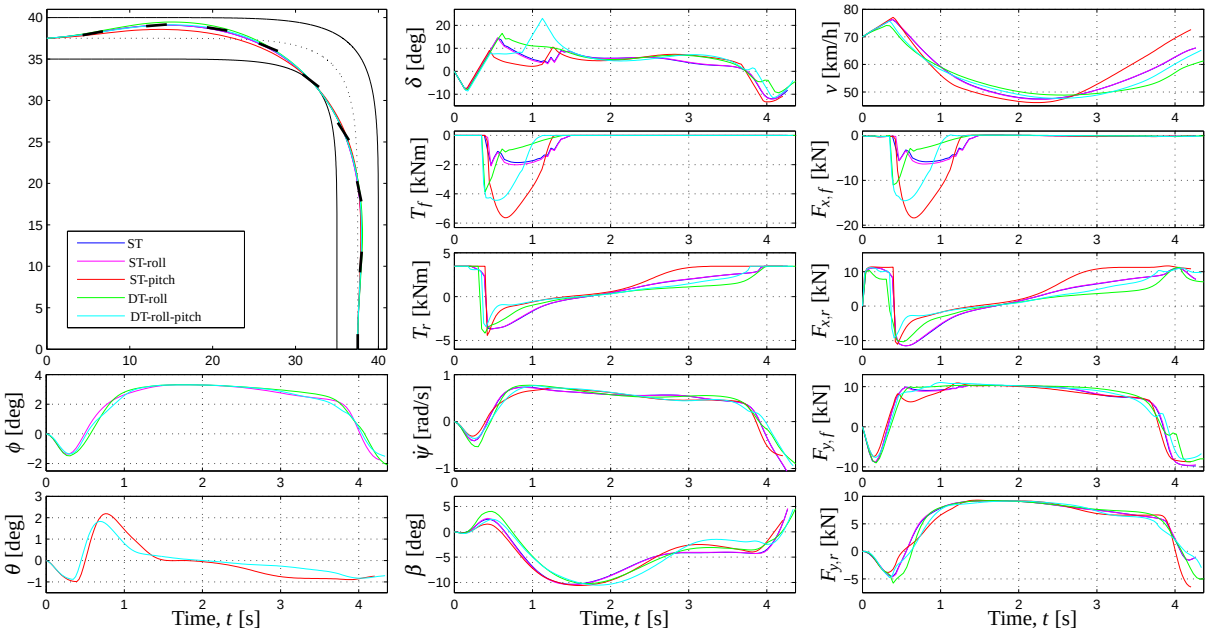

Figure 3 Time-optimal solutions obtained for the 90°-turn, for ST, ST-roll, ST-pitch, DT-roll, and DT-roll-pitch. The black bars in the upper left XY-plot represent the vehicle heading for the DT-roll-pitch solution every half second.

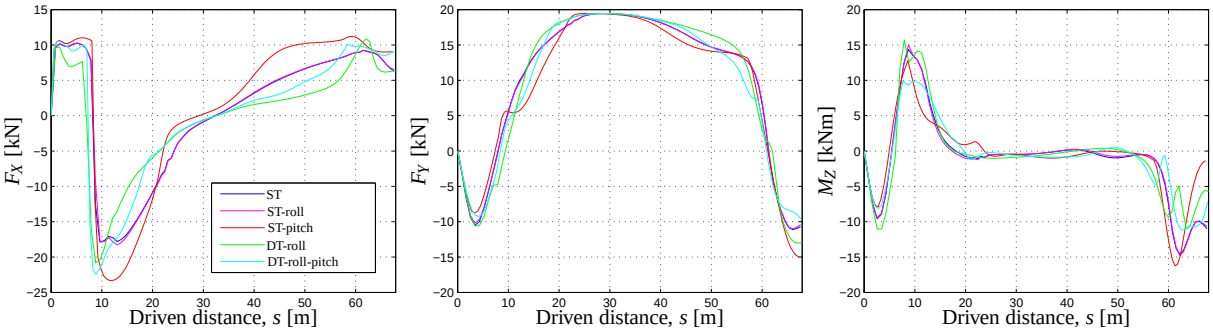

Figure 4 Longitudinal force F_X, lateral force F_Y, and yaw moment M_Z, developed by the tires, for the 90°-turn, illustrated as functions of the driven distance s. Note the similarities between the models for F_Y and M_Z.

reasons conservative bounds on the control variables might be necessary in onboard applications, consequently reducing the effects of the differences observed for the different models even further.

Investigating the results further, Figure 3 shows that the different models result in characteristics that are similar in several aspects. Prior to turning into the corner, all solutions exhibit a slight rightward maneuvering while accelerating. This is followed by a braking phase, where both front and rear wheels are used. In the braking phase, initially a significant braking torque is applied, which is gradually reduced as the vehicle approaches the turn, see T_f and T_r in Figure 3. Unsurprisingly, larger lateral forces are generated in the turn. Half-way through the turn, at $t \approx 2$ s, all solutions apply an increasing driving torque, which accelerates the vehicle out of the turn. In the final stage, maximum driving torque is applied for all models.

Differences Between the Solutions

The most prominent differences between the solutions appear for the control inputs and variables closely coupled to the longitudinal dynamics, such as T_f, T_r, and v in Figure 3, and F_X in Figure 4. In the initial braking phase, starting at $t \approx 0.4$ s, the chassis for ST-pitch and DT-roll-pitch are subjected to a forward load transfer. This is utilized by applying a larger braking effort at the front wheels, see T_f in Figure 3. At the rear wheels a large braking torque is initially applied for ST-pitch and DT-roll-pitch. This torque is then rapidly reduced as the longitudinal load transfer results in less load on the rear wheels, see T_r around $t = 0.5$ s in Figure 3.

Comparing ST with DT-roll, and ST-pitch with DT-roll-pitch, the double-track models reduce front-wheel braking earlier. This is a consequence of T_f being equally distributed between the front wheels for the double-track models. Thus, when braking while cornering, the inner wheels will have less load and thus risk to lock up

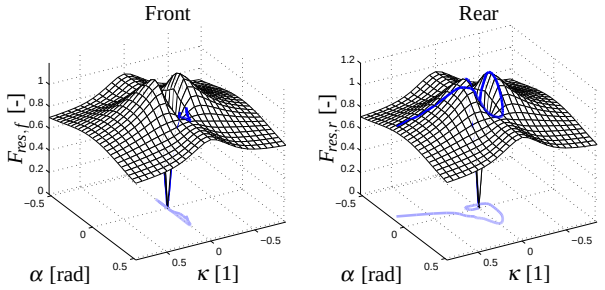

Figure 5 Resultant tire forces for ST in the 90°-turn.

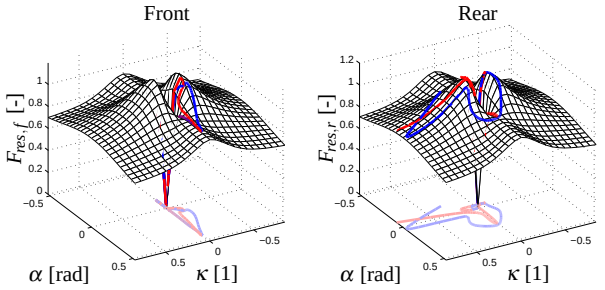

Figure 6 Resultant tire forces for DT-roll-pitch in the 90°-turn (blue–left wheel, red–right wheel).

for large braking torques. Similarly, during the exit phase where lateral load transfer still is present, a too large driving torque will spin out the inner rear wheel. Therefore, a smaller driving torque is applied for DT-roll and DT-roll-pitch compared to ST, ST-roll, and ST-pitch.

In Figure 3, the steer angle varies between the models. At $t \approx 0.7$ s, a smaller δ is obtained for ST-pitch and DT-roll-pitch, since the sought lateral force $F_{y,f}$ for the current levels of front load and braking effort requires a different slip angle α_f. Also, for ST-pitch a strategy with more emphasis on braking is obtained, with the lateral force being slightly smaller. Hence, a lower δ is natural. Shortly after, sharp peaks are seen in the steer angle for ST-pitch and DT-roll-pitch around $t = 1.1$ s. Considering the resulting forces developed at the front wheels at this time resolved in the chassis frame, there exist two different strategies to achieve these: Either by utilizing front wheel braking together with a moderate steering angle, or by only applying a large steering angle and obtain the longitudinal contribution from $F_{y,f}\sin(\delta)$ solely. The latter seems to be what, to some extent, is utilized for ST-pitch and DT-roll-pitch, and the advantage could be a more beneficial contribution to the yaw moment. Additionally, for DT-roll-pitch, front-wheel braking could conflict with lock-up for the inner wheel, thus braking might be disfavored. However, the gain in final time of using either of the strategies seems to be minor.

The FS-diagrams in Figure 5–6 display slightly different slip characteristics for the two models. For ST, the solver chooses the slip quantities to reside closer to the coordinate axes, especially for the front wheel. The DT-roll-pitch model, having dynamically varying normal forces, exhibits different slip trajectories for the left and right wheels.

4.2 Optimal Maneuver in the Double Lane-Change

The geometric track-boundaries for the double lane-change maneuver are specified according to the standardized test ISO 3888-2 [18], often used for vehicle stability evaluations. The vehicle starts at the left-hand side of the XY-plot in Figure 7, at $(X_{p,0}, Y_{p,0}) = (0,1)$ m, with an initial velocity of $v_0 = 80$ km/h. Mid-way through, an obstacle forces the vehicle into an evasive maneuver. Finally, the vehicle rejoins the initial drive lane at the final position $(X_{p,t_f}, Y_{p,t_f}) = (61, 0.6)$ m. The initial and final vehicle heading angles were set to $\psi_0 = \psi_{t_f} = 0$. In Figure 7, the time-optimal solutions for the double lane-change maneuver are shown. In Figure 8, F_X, F_Y, and M_Z are shown as function of the driven distance s, similarly to Figure 4. In Figures 9 and 10 the FS-diagrams for the solutions obtained with the ST and DT-roll-pitch models are shown. The execution times for the different models in the double lane-change maneuver are specified in Table 5. As for the 90°-turn, the execution times are similar and differing at most by 4 %.

Similarities Between the Solutions

The global trajectories, shown in Figure 7, are almost inseparable. This is partially a consequence of the narrow path formed by the track boundaries. However, strong resemblance is also obtained for several other variables , as for example $\dot{\psi}$, β, $F_{y,f}$, and $F_{y,r}$ in Figure 7. The total lateral force F_Y, as well as the yaw moment M_Z in Figure 8,

Table 5 Time for executing the maneuver for each model configuration in the double lane-change situation.

Model	Execution time
ST	2.75 s
ST-roll	2.79 s
ST-pitch	2.68 s
DT-roll	2.79 s
DT-roll-pitch	2.75 s

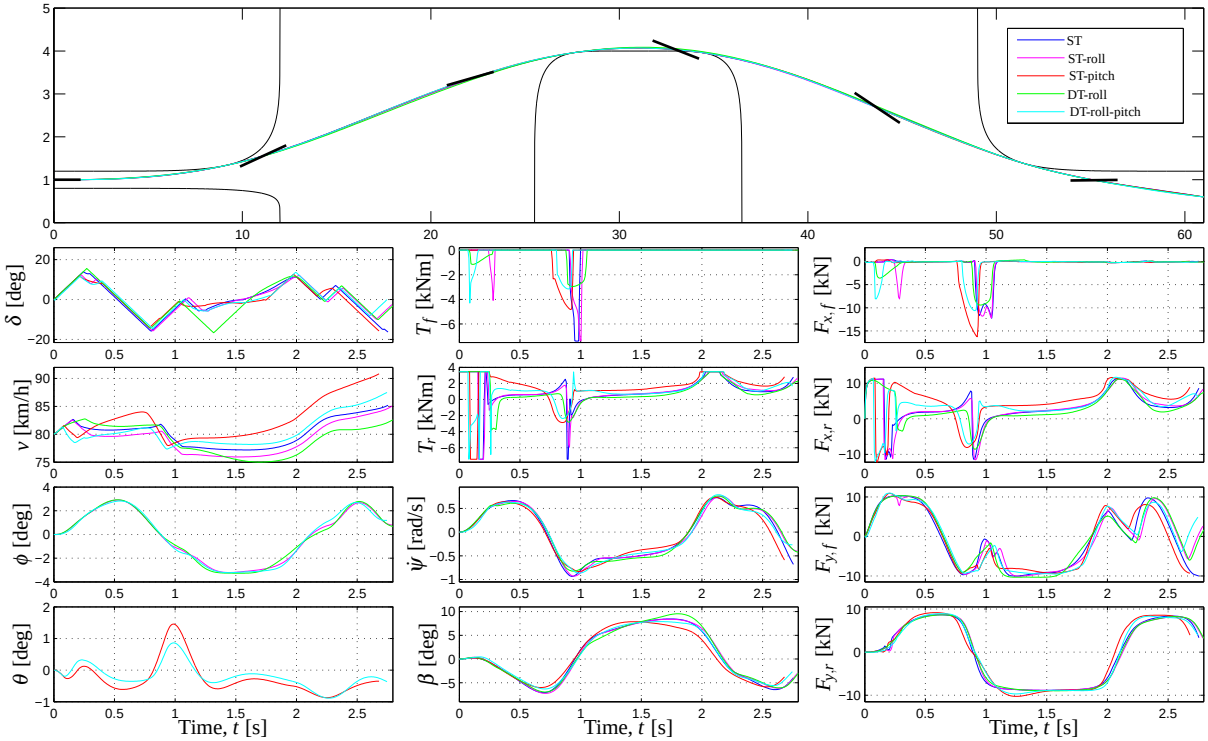

Figure 7 Time-optimal solutions for the double lane-change maneuver. Same models and color scheme as in Figure 3.

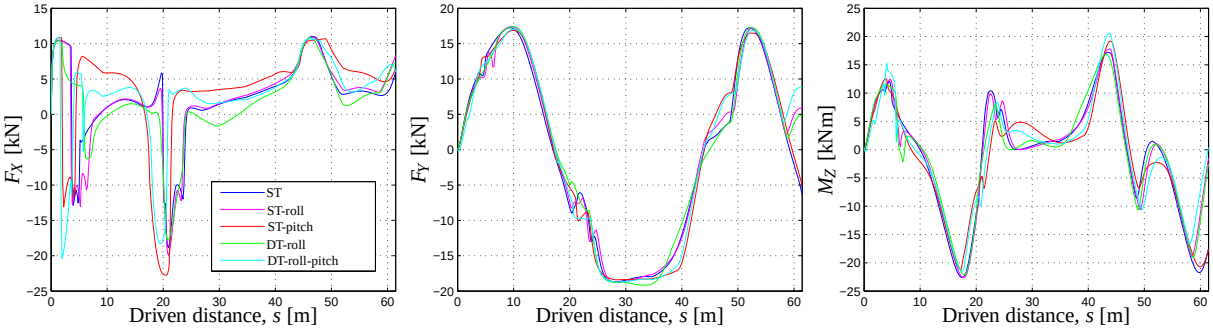

Figure 8 Longitudinal force F_X, lateral force F_Y, and yaw moment M_Z developed by the tires, for the double lane-change maneuver, illustrated as functions of the driven distance s. Note the similarities between the models for F_Y and M_Z.

show very similar behavior, almost coinciding for the main parts of the maneuver. Note the similarities in F_Y and M_Z even for considerable differences in F_X, for example around $s = 10$ m.

Analyzing the solutions more in-depth, all models result in full driving torque during the initial stage, followed by a short braking phase at the rear wheels, see T_r in Figure 7. Subsequently, various levels of driving torque are applied when approaching the obstacle, followed by a braking phase utilizing both front and rear wheel braking. For the second half of the maneuver, similar strategies are seen for all models. A moderate driving torque is applied, interrupted by a smooth but significant increase at $t = 2$ s. At this stage the rear lateral force $F_{y,r}$ shifts from negative to positive, thus only using a portion of the available lateral tire-force $\mu_{y,r}F_{z,r}$. Consequently, a longitudinal force is employed without adversely affecting the lateral forces.

Differences Between the Solutions

As for the 90°-turn, differences between the solutions are most visible in the longitudinal dynamics. This is particularly noticeable for the wheel torques, T_f and T_r in Figure 7, differing both in magnitude and point of operation. In the initial braking phase, the braking effort is slowly reduced for ST, ST-roll, and DT-roll, *i.e.*, the models without pitch dynamics, and eventually a modest driving torque is applied, see T_r in Figure 7. The models with pitch dynamics (ST-pitch and DT-roll-pitch) instead result in a maneuvering that shortly regain a driving

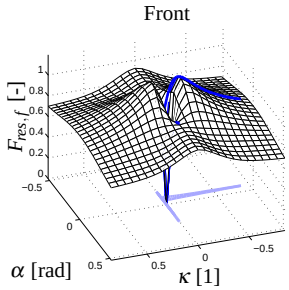

Figure 9 Resultant tire forces for ST in the double lane-change maneuver.

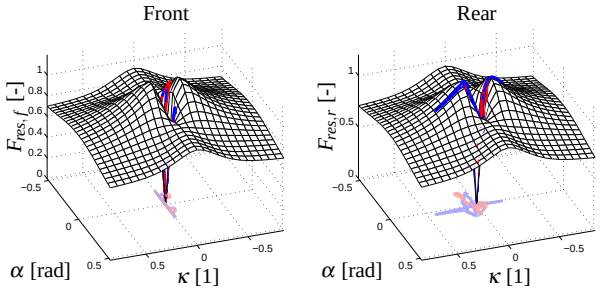

Figure 10 Resultant tire forces for DT-roll-pitch in the double lane-change (blue–left wheel, red–right wheel).

torque, which then slowly is reduced. In the pitch-dynamics models, the rearward load transfer is here utilized, enabling larger rear-wheel tire-forces because of the increased normal load on the rear wheels. Approaching the obstacle, the pitch-dynamics models show an earlier initiated braking phase, presumably because of their larger velocity. For the models without pitch dynamics, a driving torque at the rear wheels is shortly applied, followed by a very short rear-wheel braking around $t = 0.9$ s in Figure 7. The reason for this behavior is probably linked to the increased yaw rate, where a reduced rear-wheel lateral tire-force $F_{y,r}$ is desired. This can here be achieved by acquiring a large longitudinal slip.

The steering angle δ in Figure 7 exhibits overall equivalent behavior throughout the maneuver for the different models, with the steer rate-of-change limit $\dot{\delta}_{max}$ being active during a majority of the maneuver. However, at $t = 1.3$ s a distinct peak appears for DT-roll solely. This seems—as was discussed for ST-pitch and DT-roll-pitch in the 90°-turn—to be a consequence of the existence of two different strategies resulting in equivalent optimization objective. Instead of braking the front wheel, for DT-roll a large steering angle can be observed which result in a braking component determined by $F_{y,f}\sin(\delta)$. By this strategy, combined with a double-track model, a large front lateral force can be realized, while simultaneously reducing the speed without the risk of wheel lock-up. For DT-roll-pitch this strategy is not applied, since reducing the speed at this point in time seems to be neither necessary nor desired, when analyzing T_f and T_r. For the single-track models, the risk of wheel lock-up is in this situation not imminent. Hence, the absence of the large steer-angle strategy.

Investigating the FS-diagrams for the solutions for ST and DT-roll-pitch, displayed in Figures 9 and 10, the solutions exhibit a quite narrow area of operation in the α-κ plane. Also, combined slip is not utilized to the same extent as for the 90°-turn. Observing the slip trajectories closer, the rear wheels exhibit larger slip values than the front wheels, in particular for DT-roll-pitch. This is coupled to the time-critical nature of the maneuver, which becomes even more significant for DT-roll-pitch, which has dynamic normal loads.

5. CONCLUSIONS

Five different vehicle motion models were considered, ranging from a single-track model to a double-track model with roll and pitch dynamics including load transfer. These models were investigated in a 90°-turn and a double lane-change maneuver, and the optimal control problems for finding the minimum-time solution in each case were solved.

The solution behavior for the different models is similar in several key aspects for both maneuvers, as observed in Figures 3 and 7. For example, variables often used in safety systems, such as the yaw rate, the slip angle, and the roll angle, only exhibit minor discrepancies. The input torques differ significantly during parts of the maneuver. However, the overall lateral forces and yaw moments generated by the tires—F_Y and M_Z in Figures 4 and 8—for the different models have similar characteristics, with only quantitative differences in between. The largest discrepancies occur in the longitudinal forces; in Figure 8 the largest difference in absolute value of the longitudinal force between ST and DT-roll-pitch is approximately 50 %. However, this major difference is only seen for shorter time intervals and does not have much impact on the other variables. Moreover, considering an online implementation, torque and force bounds have to be set conservatively because of uncertainty in model parameters and disregarded dynamics, which will suppress this difference.

All of these observations are important, since they imply that variables traditionally considered as high-level inputs in safety systems, such as M_Z, may be generated by optimization using models with low complexity, *e.g.*, the single-track model. These high-level inputs can then be utilized as inputs to a low-level optimizer, which benefit more from complex models for distributing the desired torque to the respective wheel. This fact, together with the increased amount of sensor data and computational power available in modern road vehicles, opens up for the use of simplistic models when designing the onboard optimization-based safety systems of tomorrow.

References

[1] R. S. Sharp and H. Peng, "Vehicle dynamics applications of optimal control theory," *Vehicle System Dynamics*, vol. 49, no. 7, pp. 1073–1111, 2011.

[2] K. Berntorp, B. Olofsson, K. Lundahl, B. Bernhardsson, and L. Nielsen, "Models and methodology for optimal vehicle maneuvers applied to a hairpin turn," in *Am. Control Conf. (ACC)*, (Washington, DC), pp. 2142–2149, 2013.

[3] B. Olofsson, K. Lundahl, K. Berntorp, and L. Nielsen, "An investigation of optimal vehicle maneuvers for different road conditions," in *7th IFAC Symp. on Advances in Automotive Control (AAC)*, (Tokyo, Japan), 2013. *Accepted*.

[4] D. P. Kelly and R. S. Sharp, "Time-optimal control of the race car: a numerical method to emulate the ideal driver," *Vehicle System Dynamics*, vol. 48, no. 12, pp. 1461–1474, 2010.

[5] E. Velenis and P. Tsiotras, "Minimum time vs. maximum exit velocity path optimization during cornering," in *IEEE Int. Symp. on Industrial Electronics (ISIE)*, (Dubrovnik, Croatia), pp. 355–360, June 2005.

[6] I. Chakraborty, P. Tsiotras, and J. Lu, "Vehicle posture control through aggressive maneuvering for mitigation of T-bone collisions," in *IEEE Conf. on Decision and Control (CDC)*, (Orlando, FL), pp. 3264–3269, 2011.

[7] P. Sundström, M. Jonasson, J. Andreasson, A. Stensson Trigell, and B. Jacobsson, "Path and control optimisation for over-actuated vehicles in two safety-critical maneuvers," in *10th Int. Symp. on Advanced Vehicle Control (AVEC)*, (Loughborough, United Kingdom), 2010.

[8] J. Andreasson, "Enhancing active safety by extending controllability — How much can be gained?," in *IEEE Intelligent Vehicles Symp.*, (Xi'an, Shaanxi, China), pp. 658–662, June 2009.

[9] H. B. Pacejka, *Tyre and Vehicle Dynamics*. Oxford, United Kingdom: Butterworth-Heinemann, second ed., 2006.

[10] U. Kiencke and L. Nielsen, *Automotive Control Systems—For Engine, Driveline and Vehicle*. Berlin Heidelberg: Springer-Verlag, second ed., 2005.

[11] R. Isermann, *Fahrdynamik-Regelung: Modellbildung, Fahrerassistenzsysteme, Mechatronik*. Wiesbaden, Germany: Vieweg-Verlag, 2006.

[12] K. Berntorp, "Derivation of a six degrees-of-freedom ground-vehicle model for automotive applications," Technical Report ISRN LUTFD2/TFRT--7627--SE, Department of Automatic Control, Lund University, Sweden, Feb. 2013.

[13] Modelica Association, 2012. URL: http://www.modelica.org.

[14] J. Åkesson, K.-E. Årzén, M. Gäfvert, T. Bergdahl, and H. Tummescheit, "Modeling and optimization with Optimica and JModelica.org—Languages and tools for solving large-scale dynamic optimization problems," *Computers and Chemical Engineering*, vol. 34, pp. 1737–1749, Nov. 2010.

[15] L. T. Biegler, A. M. Cervantes, and A. Wächter, "Advances in simultaneous strategies for dynamic process optimization," *Chemical Engineering Science*, vol. 57, pp. 575–593, 2002.

[16] A. Wächter and L. T. Biegler, "On the implementation of an interior-point filter line-search algorithm for large-scale nonlinear programming," *Mathematical Programming*, vol. 106, no. 1, pp. 25–57, 2006.

[17] A. Griewank, "Evaluating derivatives: Principles and techniques of algorithmic differentiation," *Frontiers in Applied Mathematics, SIAM*, vol. 19, 2000.

[18] ISO 3888-2:2011, *Passenger cars — Test track for a severe lane-change manoeuvre — Part 2: Obstacle avoidance*. Geneva, Switzerland: International Organization for Standardization, 2011.